Minimization of out-of-plane losses of photonic crystal membranes

Rumen Iliew,[1,][*] Christoph Etrich,[2] Thomas Pertsch,[2] and Falk Lederer[1]

[1]*Institute of Condensed Matter Theory and Solid State Optics, Friedrich-Schiller-Universität Jena,*
Max-Wien-Platz 1, 07743 Jena, Germany
[2]*Institute of Applied Physics/Ultra Optics, Friedrich-Schiller-Universität Jena, Max-Wien-Platz 1, 07743 Jena, Germany*

We study in detail out-of-plane losses of photonic crystal membranes located at optical distance above a substrate by using approximate and rigorous methods. We reveal a resonance mechanism in the air gap, separating membrane and substrate being responsible for a nonmonotonic loss dependence on wavelength and gap width. We show that by taking advantage of this effect and by carefully adjusting the gap width, the losses can be even lesser than those for an isolated membrane.

I. INTRODUCTION

Photonic crystals (PhCs) with their ability to control the light propagation to a large extent have attracted a great deal of interest in the past decade. With the advances in semiconductor microstructuring technology driven by microelectronics, the fabrication of integrated optical circuits and PhCs in semiconductors has reached a rather mature level. PhC geometries particularly well adapted to this wafer-based technology are slab based,[1] i.e., the vertical light confinement is achieved in a slab waveguide utilizing total internal reflection (TIR). Recently, there was some emphasis on nonlinear interactions in semiconductor PhCs, as the Kerr effect, carrier-induced index changes, or thermo-optic effects.[2–6] The recent advances in fabricating high-index contrast microstructures in lithium niobate[7–12] (LiNbO$_3$) made slab-based PhCs available in this material system with a large quadratic nonlinearity. This renewed attention toward quadratically nonlinear interactions in two-dimensional (2D) PhCs led to recent theoretical as well as experimental investigations of optical parametric interactions[13–17] and the electro-optic tunability of the linear properties.[11,18,19] Particularly interesting is the feasibility of fabricating periodically patterned thin membranes of lithium niobate[12] which provides the benefits associated with the strong vertical guidance. However, since the membrane is usually produced by underetching of a thicker wafer, it is usually suspended over a substrate of the same material, separated from it via an air gap of a certain width.

Since the strength of nonlinear effects depends on the magnitude of the electric field, the control of losses plays a critical role for nonlinear PhCs. One feature of slab-based PhCs is the radiation loss to the substrate for operation inside the lightcone,[1,20] even in ideal structures. In a symmetric homogeneous slab waveguide, the fundamental TE and TM waveguide modes have no cut off, i.e., they are truly guided by TIR (they are outside the lightcone of the surrounding medium) and lossless for all frequencies (in absorptionless media). However, if this membrane is brought into optical proximity to a (virtually infinitely) thick substrate of the same material, light can tunnel through the respective air gap and the waveguide modes become leaky leading to propagation losses. This loss monotonically increases with decreasing distance to the substrate.

For the Bloch modes of the PhC slab the situation is different. Due to interaction with lattice vectors from the in-plane reciprocal lattice, the original wave vector of the truly guided waveguide mode may be backfolded to much smaller wavevectors inside the lightcone whose associated plane waves violate the TIR condition. This leads to radiative (out-of-plane) losses of the respective Bloch modes, even without the close proximity of a substrate. On the other hand, these radiative parts can be backreflected by a properly placed substrate, which was already utilized for reducing the losses in PhC slabs.[21–24] To enhance the reflectivity, layered substrates exhibiting Bragg reflection were used leading to a kind of antiresonant reflecting optical waveguide[25] in the vertical direction. However, the frequency dependence of the propagation losses and the actual dependence on the air-gap width were not yet systematically investigated and thus no optimization strategy has been derived. In layered semiconductor heterostructures though, where the index contrast between consecutive layers is small, the design of the complete vertical layer system was systematically studied[26] to obtain an optimal confinement strength in the guiding layer for minimum radiation losses. But the mechanisms employed there are completely different from our approach using a fixed membrane height and a reflecting substrate, as they rely on the fact that a flatter mode profile in a thick core layer may reduce the radiation loss.

In this contribution, we present an approximate method for obtaining the out-of-plane propagation losses in PhC slabs from standard numerical methods and check its validity against well-known results. Then, using this scheme we investigate the dependence of the loss spectrum on the air-gap width between a LiNbO$_3$ membrane and the LiNbO$_3$ substrate because this structure is readily available with current technology and the width of the gap is a technologically critical point. Depending on the actual PhC structure, we optimize the thickness of the air gap for loss minimization.

Different methods for obtaining the loss spectrum for propagation of butt-coupled light in PhCs were proposed. The finite-difference time-domain (FDTD) method,[27] one of the most popular methods for simulating light propagation in photonic devices, has been widely used to obtain transmission spectra.[28–34] For that purpose, the spectrally resolved fluxes of the time-averaged Poynting vector at the output and the input are set in relation to each other. To obtain the pure

propagation loss spectrum without parasitic Fabry-Pérot ripples caused by reflections at the end of the computational window, different means of terminating it were proposed.[35,36] However, for slow light, which is an important aspect of using PhC waveguides, avoiding reflections becomes increasingly difficult. Furthermore, isolating a particular mode of a multimode waveguide is relatively complicated as the excitation must match the modal cross section over a wide spectral range. One multistep solution for obtaining losses for higher-order modes at a previously fixed frequency with the FDTD method is described in Ref. [31], where the complete field of a multimode excitation is projected onto the (previously determined) fields of the individual modes at this frequency for different propagation lengths.

A method where these problems do not arise is the Fourier modal method, where the complex Bloch vector in propagation direction for all individual waveguide modes is obtained for a given frequency.[37] As the imaginary part of this Bloch vector describes the attenuation of the Bloch mode in propagation direction, it is a direct measure for the propagation losses. However, this method requires the solution of a large generalized eigenvalue problem. Another method that calculates the complex Bloch vector based on finite differences is given in Ref. [38]. A very efficient perturbative method based on the expansion of the fields by means of the modes of the unstructured slab waveguide was proposed in Ref. [39]. It calculates the band structure, i.e., the complex frequency for a given real Bloch vector of PhC slabs at low computational costs. Also, standard methods, such as the finite-element method (FEM) (Ref. [40]) or the finite-difference frequency-domain method,[41] give the complex frequency for a fixed real Bloch vector instead of a complex component of the Bloch vector for a real frequency. The formula for calculating the propagation losses from the complex eigenfrequency in PhCs (Refs. [42–45]) was originally used for laser cavities,[46,47] where the cavity was assumed to be a longitudinally homogeneous waveguide. However, there is no proper derivation for periodic structures. Therefore, it is the aim of this paper to introduce a perturbation approach that allows us to readily obtain the imaginary part of the Bloch vector in a given direction from this complex frequency and to subsequently evaluate and minimize the propagation losses.

The rest of the paper is structured as follows. In Sec. II the perturbation approach for obtaining the propagation loss is presented. The radiation-induced losses for a W1 waveguide in a silicon membrane are calculated and verified by means of previously published results. In Sec. III we formulate an antiresonance condition for obtaining maximum back reflection of radiation leaving the membrane. Using the dispersion relation of a W1 waveguide in a LiNbO$_3$ membrane, we propose frequency regions of lowest radiation losses for different gap widths. In Sec. IV the loss spectra for a W1 waveguide in a LiNbO$_3$ membrane are calculated by means of the presented perturbation method in dependence on the air-gap width. These are compared to the results obtained from the antiresonance condition. Finally we conclude the paper.

II. PERTURBATION THEORY FOR CALCULATION OF PROPAGATION LOSSES

The subject of the following analysis are the eigenmodes of a 2D or one-dimensional periodic photonic crystal slab,[1] where the guidance in the vertical direction (z) is provided by TIR of a slab waveguide structure. Using the Bloch theorem, the eigenmodes of this system can be written in the time domain as

$$\mathbf{E}(\mathbf{r},t) = \frac{1}{2}\mathbf{e}_{n\mathbf{k}}(\mathbf{r})\exp(\iota\mathbf{k}\cdot\mathbf{r}^{(2)})\exp(-\iota\omega_n t) + \text{c.c.}, \quad (1a)$$

$$\mathbf{H}(\mathbf{r},t) = \frac{1}{2}\mathbf{h}_{n\mathbf{k}}(\mathbf{r})\exp(\iota\mathbf{k}\cdot\mathbf{r}^{(2)})\exp(-\iota\omega_n t) + \text{c.c.}, \quad (1b)$$

where $\mathbf{e}_{n\mathbf{k}}(\mathbf{r})$ and $\mathbf{h}_{n\mathbf{k}}(\mathbf{r})$ are the Bloch amplitudes which are periodic on the 2D lattice and decay (or possibly leak) into the z direction, $\mathbf{k} = (k_\parallel, k_\perp)$ and $\mathbf{r}^{(2)} = (r_\parallel, r_\perp)$ are the 2D Bloch vector and 2D position in the plane of periodicity, respectively, where $\parallel$ denotes the component in the direction (energy transport) of propagation and $\perp$ the component perpendicular to this direction, and n is the band index, i.e., counts the eigenmodes for fixed $\mathbf{k}$. Due to the missing periodicity in the vertical direction (z, direction of radiation) no Bloch vector component can be defined here.

We are interested in the regime inside the lightcone where, due to the unavoidable coupling to radiation modes (exceptions due to symmetries may occur[48]), no truly guided modes exist. Instead, the modes can be described in the leaky-mode picture, where the only modification to Eqs. (1) is the necessary introduction of complex eigenvalues. Different formulations are possible in this case. We deal with the two most common formulations in the following denoted by the superscripts "I" and "II." The first formulation considers a real 2D Bloch vector $\mathbf{k}$ and solves for the complex eigenfrequency $\omega_n = \omega_n' - \iota\gamma_n/2$ with ω_n' and γ_n both being real and positive. As already mentioned, different computational methods allow for obtaining the eigenvalues $\omega_n(\mathbf{k})$ and the modal fields. A physical realization would be a cavity of the size of one unit cell (UC) with the appropriate 2D Bloch boundary conditions that is uniformly excited and where the stored energy decays in time proportional to $\exp(-\gamma_n t)$. The second formulation starts from a fixed real frequency and one real component $k_\perp$ of the Bloch vector and yields an eigenvalue problem for the complex second component of the Bloch vector $k_\parallel = k' + \iota\alpha_n/2$ (k' and α_n are real, and α_n is positive) in Eqs. (1). Physically this corresponds to a homogeneous (Bloch periodic in one dimension only) continuous-wave (CW) excitation at one facet of the PhC slab along the $\perp$ direction, where the guided power decays along the propagation in $\parallel$ direction proportional to $\exp(-\alpha_n r_\parallel)$.

The goal of the perturbation theory derived below is to obtain a relation between γ_n and α_n which, e.g., permits us to determine the propagation losses from the complex eigenfrequency analysis in a truly Bloch periodic unit cell. In the case of 2D periodic boundaries, the same amount of energy W is stored at any moment in the individual unit cells in the 2D plane while the fields homogeneously radiate into the cladding and/or substrate. Due to this radiative energy loss

per unit cell given by the flux of the time-averaged Poynting vector through the top (A_t) and bottom (A_b) surfaces of one unit cell

$$-\frac{dW}{dt} = \int_{A_t \cup A_b} dA \, \mathbf{S}^I \cdot \mathbf{n}, \qquad (2)$$

the stored amount of energy decreases exponentially in time, $W(t) = W(0)\exp(-\gamma_n t)$. In Eq. (2), $\mathbf{S}^I = \langle \mathbf{E}(t) \times \mathbf{H}(t) \rangle$ is the time-averaged Poynting vector, where $\mathbf{E}(t)$ und $\mathbf{H}(t)$ are the real fields in time domain and $\mathbf{n}$ is the (position-dependent) unit vector normal to the surface pointing away from the structure. Denoting these complex modal fields (Bloch modes) by $\mathbf{e}_{n\mathbf{k}}^I(\mathbf{r})$ and $\mathbf{h}_{n\mathbf{k}}^I(\mathbf{r})$, we obtain $\mathbf{S}^I = \mathrm{Re}[\mathbf{e}_{n\mathbf{k}}^I \times (\mathbf{h}_{n\mathbf{k}}^I)^*]\exp(-\gamma_n t)/2$. The superscript I indicates here the fields in the first formulation, which are 2D Bloch periodic and decay exponentially in time. The fields $\mathbf{e}_{n\mathbf{k}}^I$ and $\mathbf{h}_{n\mathbf{k}}^I$, with the corresponding complex frequency $\omega_n(\mathbf{k})$, result from standard eigenvalue solvers imposing Bloch periodic boundary conditions on the unit cell and open boundaries at the appropriate faces and solving for the complex eigenfrequency.

On the other hand, if a certain Bloch mode is excited with a CW source at one end of the PhC, the temporal behavior of the complete field is fixed and nondecaying. Thus the transverse field distribution is a Bloch periodic one ($k_\perp$ is real). Since losses still occur due to radiation into the substrate and/or cladding, the field amplitude decays with increasing distance from the excitation. The power

$$P_{\mathrm{rad}}(r_\parallel) = \int_{A_t \cup A_b} dA \, \mathbf{S}^{II} \cdot \mathbf{n} \qquad (3)$$

radiated by one unit cell (extension $a_\parallel$ in propagation direction) at position $r_\parallel$ leads to an equivalent decrease in the guided power

$$P(r_\parallel) = \int_{A_\parallel} dA \, \mathbf{S}^{II} \cdot \mathbf{n} \qquad (4)$$

upon propagation to the next unit cell. Here $A_\parallel$ is the unit-cell cross section (surface normal in direction $\parallel$). The superscript II reminds us that these are the fields obtained for a true CW time dependence which are (spatially) decaying along $r_\parallel$. Due to the exponential decay of the fields, the guided power behaves along propagation as $P(ma_\parallel) = P(0)\exp(-m\alpha_n a_\parallel)$ with α_n being the (yet unknown) loss coefficient and m a positive integer. The energy balance for propagation along one period $a_\parallel$ in propagation direction is now $P_{\mathrm{rad}}(r_\parallel) = P(r_\parallel)[1 - \exp(-\alpha_n a_\parallel)]$. For $\alpha_n a_\parallel \ll 1$, we further obtain

$$P_{\mathrm{rad}}(r_\parallel) \approx \alpha_n a_\parallel P(r_\parallel). \qquad (5)$$

In order to establish a relation between these two physically different settings and the respective decay constants γ_n and α_n, we assume that the complex Bloch fields $(\mathbf{e}_{n\mathbf{k}}^I, \mathbf{h}_{n\mathbf{k}}^I)$ and $(\mathbf{e}_{n\mathbf{k}}^{II}, \mathbf{h}_{n\mathbf{k}}^{II})$ do not differ substantially meaning that the radiated powers per unit cell [right-hand side of Eqs. (2) and (3)] are equal. Hence, together with Eq. (5) we obtain $\alpha_n a_\parallel P(r_\parallel=0) = \gamma_n W(t=0)$. The relation between the power guided in a certain direction (here $\parallel$) averaged over one unit

cell with period $a_\parallel$ in the propagation direction and the total electromagnetic energy in this unit cell is given by the group velocity in the respective direction[49]

$$v_{g\parallel} = \frac{\dfrac{1}{2}\displaystyle\int_{UC} d^3\mathbf{r} \, \mathrm{Re}[\mathbf{e}_{n\mathbf{k}}(\mathbf{r}) \times \mathbf{h}_{n\mathbf{k}}^*(\mathbf{r})]_\parallel}{\dfrac{1}{4}\displaystyle\int_{UC} d^3\mathbf{r}[\varepsilon_0 \varepsilon(\mathbf{r})|\mathbf{e}_{n\mathbf{k}}(\mathbf{r})|^2 + \mu_0|\mathbf{h}_{n\mathbf{k}}(\mathbf{r})|^2]}. \qquad (6)$$

From Ref. 50 the numerator is $a_\parallel P(r_\parallel=0)$. The denominator is $W(t=0)$. With the previous assumption that the Bloch amplitudes in both formulations do not substantially differ, we finally obtain

$$\alpha_n = \frac{1}{v_{g\parallel}}\gamma_n = \frac{2}{v_{g\parallel}}\mathrm{Im}\,\omega_n(\mathbf{k}), \qquad (7)$$

or, using the definition of the quality factor $Q_n = \omega_n'/\gamma_n$ of a cavity, $\alpha_n = \omega_n'/Q_n v_{g\parallel}$.

In practice, however, the mode solver provides the complete modal fields $\mathbf{e}_{n\mathbf{k}}(\mathbf{r})$ and $\mathbf{h}_{n\mathbf{k}}(\mathbf{r})$, and usually Eq. (6) is directly used to compute the group velocity instead of calculating the first derivative $\partial\omega'/\partial k_\parallel$ of the dispersion relation. This also means that the propagation losses can be obtained by exclusively solving the eigenvalue problem for *one* Bloch vector alone. We used a commercial FEM solver (COMSOL Multiphysics by COMSOL AB, http://www.comsol.com/) to calculate the complex eigenfrequencies for one unit cell with periodic boundary conditions in the plane and perfectly matched layer (PML) boundary conditions in the vertical direction in order to allow the radiation to leave the finite computational domain without reflection. For the case of PhC line defect waveguides, where only periodicity in one dimension is left, we used PML boundaries also in the in-plane direction perpendicular to the waveguide. In order to reduce the computational cost, we utilized the mirror symmetry of the waveguide system with respect to the plane $y=0$. For the pure membrane also the mirror symmetry around $z=0$ can be exploited gaining another factor of 2.

Now we are going to evaluate the performance of this approximation in calculating the loss spectrum and comparing it with the results of Ref. 43. To this end we use the same sample, namely, a W1 waveguide in a silicon PhC membrane, as shown in Fig. 1. Line-defect PhC waveguides are primary components of PhC circuits, since they allow for unusual optical properties such as tuning of the dispersion to a wide extent.[51–53] With the current fabrication technology, air hole structures in a dielectric background are most commonly experimentally investigated. Such periodic structures favor TE bandgaps in genuine 2D systems and bandgaps for TE-like light in PhC membranes.[1] For the fundamental mode of the slab waveguide TE-like means here that the (vectorial) electric field is even with respect to the mirror-symmetry plane $z=0$ in the center of the membrane. For higher-order slab modes, this parity of TE-like and TM-like can change.[48] Since we are only interested in thin slabs which are single mode in the frequency range of interest, higher-order slab modes can be disregarded here. In the following, we will focus on a hexagonal lattice of circular air holes because it
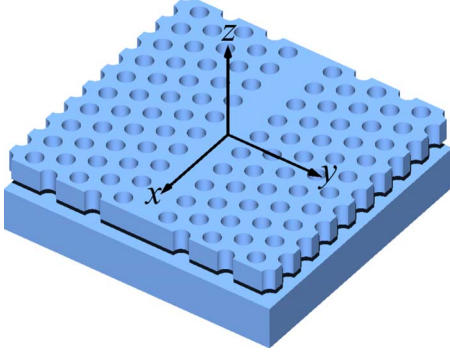
FIG. 1. (Color online) A W1 waveguide in a PhC membrane suspended at a finite distance over a dielectric substrate and the coordinate system used.

FIG. 2. Dispersion relation and normalized attenuation length (of the main branch of the mode denoted by A_n) of the membrane W1 waveguide decribed in the text. Here and in the following, the gray regions in the dispersion relation correspond to the continuum of two-dimensional Bloch modes of the underlying periodic PhC structure.

usually yields the largest bandgaps (for TE-like light). Hence, we restrict the following analysis to TE-like light. A W1 defect waveguide is introduced by omitting one row of holes in ΓK direction.

A major issue with these waveguides is lightcone radiation losses, also referred to as intrinsic diffraction losses. This applies even to ideal structures (no roughness and truly periodic). In the following, we calculate the dispersion relation and the losses of a prototypical system investigated in Ref. 43. The results are compared to those obtained with the guided-mode expansion (GME) method introduced in this reference.

The structure investigated is a W1 waveguide in a patterned silicon membrane (without substrate) with a dielectric constant $\varepsilon=12$ and a thickness $d=0.3a$, where a is the lattice constant of the hexagonal air hole lattice and $r=0.36a$ is the hole radius. For the infinite purely periodic PhC membrane, this leads to a photonic bandgap for TE-like modes in the frequency region $0.326<\omega'a/2\pi c<0.456$, where due to the relatively small thickness $d<\lambda/7$ the vertical confinement is weak.

We utilize the mirror symmetries in the vertical (z) and in the transverse horizontal (y direction) to reduce the size of the simulated structure by a factor of 4. Bloch periodic boundary conditions are used in waveguide (x) direction and PML boundaries in the y and z directions.

The dispersion relation and the attenuation length $\mathcal{L}$ $=1/\alpha_n$ obtained for this membrane are shown in Fig. 2. Only the modes which are odd with respect to the mirror plane y $=0$ are shown. In the following, we call modes with this symmetry simply odd modes. The coincidence with the results obtained by the GME method can clearly be seen in comparing them with those shown in Figs. 1 and 2(c) in Ref. 43.

III. LOSS DEPENDENCE ON THE AIR-GAP WIDTH

Air suspended PhC membranes are usually fabricated using undercutting techniques. However, usually the substrate below the membrane cannot be completely removed because the membrane needs mechanical support. For certain systems, e.g., lithium niobate membranes, the width of the resulting air gap between the membrane and the substrate of
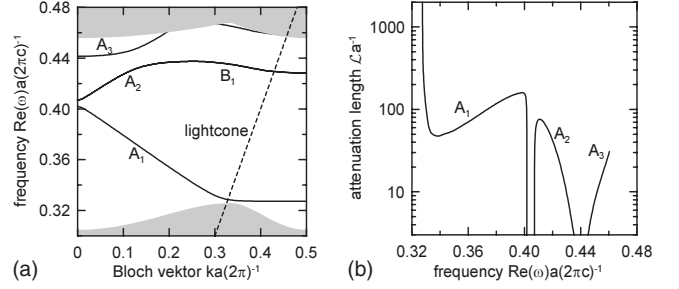
the same dielectric is a technologically critical issue. Since vertical guidance in the slab waveguide is provided by TIR (high-index membrane), it is clear that even for unstructured membranes there is no ideal confinement if an extended high-index substrate is located in close proximity to the waveguide. In the resulting air gap, the waves are still evanescent but are of radiating nature in the substrate. Hence, the air gap is merely a tunneling barrier for the light which allows for energy transport off the waveguide. These quasiguided modes can be conveniently described in the leaky-mode picture, where radiation losses lead to a complex propagation constant. Since no resonances are possible for evanescent waves in the air gap, the losses of the fundamental mode of the unstructured waveguide monotonically increase with decreasing air-gap width.

On the other hand, in the periodically structured membrane, intrinsically guided modes of the unstructured slab can couple via reciprocal-lattice vectors to radiation modes of the free space (lightcone region). In contrast to the decaying evanescent fields, this radiation traverses the air gap without attenuation, is partially reflected at the substrate interface, and is partially penetrating into the substrate, where it is ultimately lost. Due to its oscillating nature in the air gap, however, resonance features, depending on the ratio of oscillation period and gap width, are expected. Hence, for a given wavelength, the dependence of the loss on the air-gap width should be nonmonotonic. Similar to a Fabry-Pérot cavity, the best transmission of the radiation through the gap is expected for a gap width corresponding to multiples of $\pi/k_z=\lambda_z/2$ (λ_z is the wavelength of the oscillations in the z direction), whereas odd multiples of $\lambda_z/4$ should give maximum reflection and, hence, minimum radiation losses of the PhC component. This physical mechanism was utilized in earlier designs[22–24] but not systematically investigated.

In the following, we explore in detail the influence of the (anti)resonant reflection mechanism by calculating the losses of a W1 waveguide in a realistic lithium niobate PhC varying the air-gap width. First we estimate the air-gap width for achieving antiresonance, which should eventually lead to minimum PhC slab losses. Resonant coupling of a Bloch mode with Bloch vector **k** from the first Brillouin zone (BZ) to radiation in the air region with three-dimensional wave vector $(\mathbf{k}+\mathbf{G},k_z)$ occurs for frequencies for which a
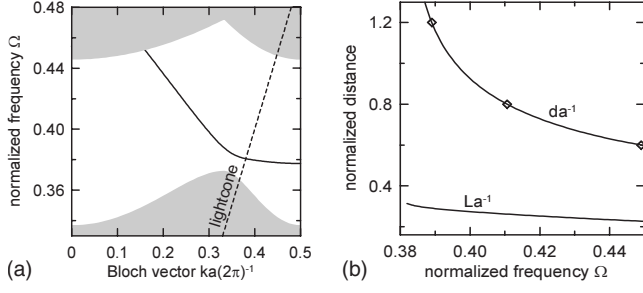
FIG. 3. Left: dispersion relation for the odd mode of the W1 waveguide in the bandgap region. Right: normalized antiresonance ($m=1$) air-gap width d/a ($G=0$) and normalized vertical decay length L/a ($G=-2\pi/a$) as functions of the normalized frequency.

reciprocal-lattice vector **G** exists, such that the free space dispersion relation

$$\left(\frac{\omega'}{c}\right)^2 \varepsilon_{\text{gap}} = (\mathbf{k}+\mathbf{G})^2 + k_z^2 \qquad (8)$$

is fulfilled. Obviously, this can only happen for frequencies above the gap light line $\omega' > |\mathbf{k}|c/\sqrt{\varepsilon_{\text{gap}}}$. The condition for antiresonance is $k_z d = m\pi/2$ with m being an odd integer, whereas, for resonance m is even. d is the air-gap width. Finally we obtain

$$\frac{d}{a} = \frac{m}{4} \frac{1}{\sqrt{\Omega^2 \varepsilon_{\text{gap}} - (\mathbf{K}+\tilde{\mathbf{G}})^2}}, \qquad (9)$$

where again we have resonance if m is even and antiresonance if m is odd. Here ε_{gap} is the dielectric function of the gap region (usually 1 for air), $\mathbf{K}=\mathbf{k}a/2\pi$ the normalized Bloch vector, $\tilde{\mathbf{G}}=\mathbf{G}a/2\pi$ the normalized reciprocal-lattice vector, and $\Omega = \omega'a/2\pi c = a/\lambda$ the normalized (real part of the) frequency.

We assume a membrane of a normalized width $h/a = 0.8333$ and a hole radius of the hexagonal lattice of $r/a = 0.3167$. We approximate the uniaxial medium as dispersionless and isotropic with $\varepsilon = 4.888521$ because the small shifts in the dispersion relation caused by the birefringence are beyond the scope of our investigation. However, when a definite design for phase-sensitive effects is needed, the birefringence and material dispersion can be easily taken into account.[17] The W1 waveguide is investigated because of its large practical importance. The dispersion relation obtained from FEM calculations is shown in Fig. 3. From calculations for different air-gap widths, we find that the vertical asymmetry introduced by placing the substrate as close as $d/a = 0.6$ to the membrane leads to relative changes of the real part of the frequency eigenvalue of at most 0.03% compared to the pure membrane case. This is in contrast to a layered PhC film system, where a high-index layer is directly deposited on a substrate of lower index.[54] Hence the result for the pure membrane can be used in the cases with a (not too close) substrate as well, without introducing a significant error. Furthermore, in the graphical presentation virtually no differences will be apparent between the dispersion relations for different gap widths. Now, according to Eq. (9) the nor-
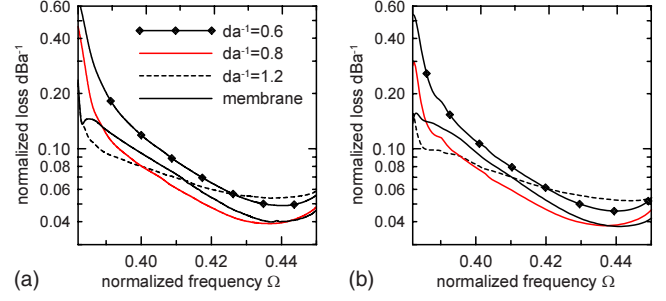
FIG. 4. (Color online) Propagation losses for the W1 waveguide as a function of the normalized frequency for different air-gap widths. Left: FDTD transmission calculations; right: approximate model based on FEM eigenmode calculations.

malized antiresonance width of lowest order ($m=1$) and for $\mathbf{G}=0$ can be calculated as a function of the operating frequency. It is depicted in Fig. 3. The normalized vertical decay length is given by

$$\frac{L}{a} = \frac{1}{a\gamma_z} = \frac{1}{2\pi} \frac{1}{\sqrt{(\mathbf{K}+\tilde{\mathbf{G}})^2 - \Omega^2 \varepsilon_{\text{gap}}}} \qquad (10)$$

for evanescent (in z direction) plane-wave components $|\mathbf{K}+\tilde{\mathbf{G}}| > \Omega\sqrt{\varepsilon_{\text{gap}}}$ of the field outside the lightcone. Here γ_z is the exponential decay constant describing the vertical damping of the field $\propto \exp(-\gamma_z z)$ in the air region. The decay length, weighted by the fraction of the respective plane-wave component of the field, is a measure for the losses induced by nonresonant tunneling into the substrate. To investigate the interplay of these two effects (tunneling and radiation through the air gap), we deal both with the isolated membrane ($d=\infty$) and three selected air-gap widths $d/a = 0.6, 0.8, 1.2$ marked by symbols in Fig. 3 and corresponding to the antiresonance frequencies $\Omega = 0.449, 0.411, 0.389$, respectively. Obviously, as long as the waveguide mode has a substantial fraction of **K** components in the first BZ $\mathbf{K} \in [-0.5, 0.5)\mathbf{e}_x$, the associated radiation to the substrate should be best reflected around these given frequencies. Here $\mathbf{e}_x$ is the unit vector in x direction (corresponding to the direction of the line defect, $\Gamma\mathbf{K}$). On the other hand, for **K** components in higher-order BZs leading to evanescent decay [positive argument of the square root in Eq. (10)] obviously the largest frequency yields the fastest decay and, hence, the weakest energy transport into the substrate via tunneling.

IV. LOSS SPECTRA FOR LINE DEFECT WAVEGUIDES

To verify the conclusions for the loss dependence on the air-gap width drawn in the previous section, the losses obtained from FDTD transmission calculations of a W1 waveguide of length $68a$ are depicted in Fig. 4. The PhC cladding on both sides of the line defect comprised ten rows of holes (in y direction). The source for creating the incident field is a Gaussian pulse with an asymmetric (elliptical) transverse profile. These exact loss results are compared to the ones obtained from the frequency eigenvalues via the approximate

Formula (7) (see Fig. 4). The frequency eigenvalues are derived from FEM calculations in the unit cell. Obviously, here is an excellent agreement between the rigorous and the approximate method.

It can be seen that the different loss curves intersect, which is a signature of the nonmonotonic and wavelength-dependent loss dependence on the air-gap width. In the frequency region around $\Omega = 0.39$, the loss for the pure membrane without substrate is significantly larger than for air-gap widths $d = 0.8a$ and $d = 1.2a$. This becomes evident because for $d = 1.2a$, the antiresonance frequency is $\Omega = 0.389$ (see Fig. 3) leading to a maximum reduction in the loss due to reflection at the substrate interface. For $d = 0.8a$, this frequency is 0.411 still reducing the loss at $\Omega = 0.39$ because the antiresonances are spectrally relatively broad. Therefore at $\Omega = 0.411$, the case $d = 0.8a$ has the minimum losses in full coincidence with our expectations outlined in the previous section. Finally, for $d = 0.6a$ with an antiresonance frequency of 0.449, the loss is at least smaller than that for $d = 0.8a$ in the frequency range around 0.44. However, there is no frequency interval where the losses are minimal for $d = 0.6a$. This is due to the second loss mechanism, the nonresonant evanescent tunneling through the air-gap, which is strongest in this case (see the vertical decay length L shown in Fig. 3).

However, it should be mentioned that the radiation leaves the system unreflected in the half space above the membrane due to the missing interface leading to unavoidable losses. Hence, the losses cannot go below a certain finite limit caused by that radiation. On the other side, there are obviously no losses related to evanescent field tunneling into this area. Thus even for modes comprising only radiative **K** vector components, at most, half of the radiation losses can be avoided by carefully adjusting the substrate.

In conclusion, for frequencies inside the lightcone, the case $d = 0.8a$ exhibits globally the lowest losses, even lower than the isolated membrane. This is due to the particular field structure of the waveguide modes with evanescent as well as radiative parts in the air gap and their different behavior with respect to the substrate.

The situation changes in a broader waveguide, e.g., a W3. There we anticipate a less pronounced resonance effect because the interaction of the field with the periodic structure is weaker and a smaller fraction of the **K** components is expected to be inside the lightcone. Hence, the width dependence of the losses should follow the monotonic behavior for slab waveguides much more. To investigate the interplay between evanescent and radiative waves in such a wider waveguide, we calculated the propagation losses for the fundamental mode in a W3 waveguide for different air-gap widths from the frequency eigenvalues obtained with the FEM by means of the approximate method. The dispersion relation (comprising the branches denoted by the number 1) and the losses are shown in Fig. 5.

One obvious feature is the low transmission around $\Omega = 0.425$, which is in stark contrast to the W1 waveguide. This strong transmission reduction is not related to the two loss mechanisms discussed previously. It is rather evoked by the existence of a so-called ministop band (MSB) (Ref. 55–57) (see Fig. 5, left) that arises as a result of avoided crossing of the fundamental index guided mode with a gap guided[51,57]
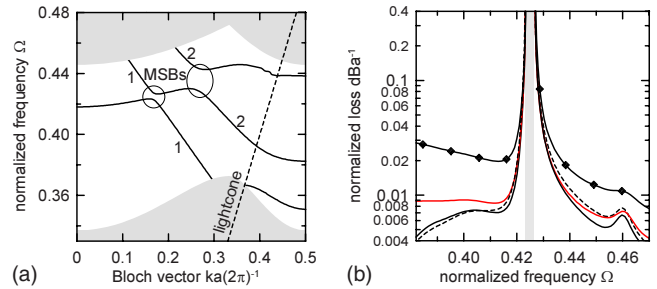
FIG. 5. (Color online) Left: Dispersion relation of the modes of interest; right: Propagation losses for the fundamental mode of a W3 waveguide as a function of the frequency and for different air-gap widths. Different lines correspond to Fig. 4. The gray region in the right graph corresponds to the MSB where the fundamental mode does not exist and, hence, the loss is undefined.

higher-order mode in the dispersion relation. In this frequency range the guided mode is rejected from the W3 waveguide. As expected, the effect of the reflecting substrate is much less pronounced leading to a monotonic loss dependence on the air-gap width. For $d = 0.6a$, the loss is substantially increased compared to all other widths for all frequencies. Due to the larger decay length at frequencies around $\Omega = 0.39$, the tunneling losses prevail. Obviously, for the W3 waveguide the conclusion can be drawn that for the fundamental mode a larger air-gap width always reduces the losses, although increasing the width to more than $1.2a$ does not significantly help. Because of their experimental relevance, we also investigate the losses of the higher-order modes as they are also usually excited, in particular, if they exhibit the same transverse symmetry as the fundamental mode. In Fig. 6, the loss of the higher-order odd mode (comprising the branches denoted by the number 2 in the left part of Fig. 5) is shown for different air-gap widths. The situation here resembles more the one of the W1 waveguide because the interaction of this broader mode with the periodic structure becomes larger again and, aside from the occurring larger MSB, out-of-plane losses increase, as already experi-
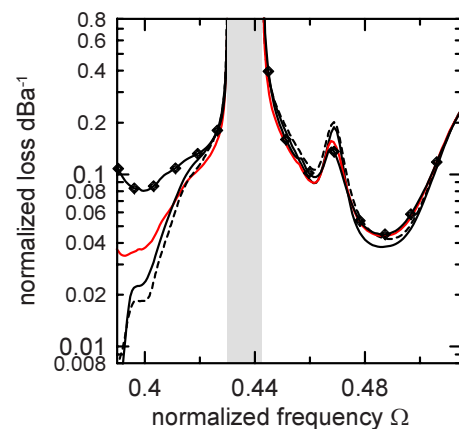
FIG. 6. (Color online) Propagation losses of the higher-order odd mode of the W3 waveguide as a function of the frequency and for diffrent air-gap widths. The different lines correspond to the legend given in Fig. 4. The gray region corresponds to the MSB where this mode does not exist and, hence, the loss is undefined.

mentally observed.[58] This leads, after a certain propagation distance, to an effective single-mode behavior as the higher-order modes suffer significantly larger losses.

V. CONCLUSIONS

We have shown that by carefully adjusting the air gap between a PhC membrane hosting a W1 waveguide and the substrate, the out-of-plane losses can be substantially reduced even below those of a free-standing membrane. The physical reason is that these losses are evoked by two effects, namely, the tunneling into the substrate and the radiation of backfolded modes into the substrate. In the PhC-substrate system, the latter effect can be almost suppressed by taking advantage of the broadband Fabry-Pérot antiresonance condition. The optimization of the structure can be performed by using an approximate method which is based on the complex-frequency eigenvalues obtained from FEM calculations with Bloch periodic in-plane boundary conditions. The results have been double checked against those obtained by using the rigorous FDTD method where excellent agreement could be shown. The method has been applied to the practically and technologically relevant system of a lithium niobate PhC slab suspended over a lithium niobate substrate. The reduction effect is less pronounced for wider waveguides where the tunneling losses are pivotal. The loss reduction mechanism is not restricted to PhC waveguides. Instead it may become relevant in designing devices utilizing unusual dispersion and diffraction phenomena in 2D periodic PhC membranes or high-Q microresonators in lithium niobate PhC membranes for miniaturized frequency converters.

*rumen.iliew@uni-jena.de

[1] S. G. Johnson, S. Fan, P. R. Villeneuve, J. D. Joannopoulos, and L. A. Kolodziejski, Phys. Rev. B **60**, 5751 (1999).

[2] P. Barclay, K. Srinivasan, and O. Painter, Opt. Express **13**, 801 (2005).

[3] M. Notomi, A. Shinya, S. Mitsugi, G. Kira, E. Kuramochi, and T. Tanabe, Opt. Express **13**, 2678 (2005).

[4] X. Yang, C. Husko, C. W. Wong, M. Yu, and D.-L. Kwong, Appl. Phys. Lett. **91**, 051113 (2007).

[5] A. Shinya, S. Matsuo, Yosia, T. Tanabe, E. Kuramochi, T. Sato, T. Kakitsuka, and M. Notomi, Opt. Express **16**, 19382 (2008).

[6] C. Monat, B. Corcoran, M. Ebnali-Heidari, C. Grillet, B. J. Eggleton, T. P. White, L. O'Faolain, and T. F. Krauss, Opt. Express **17**, 2944 (2009).

[7] F. Lacour, N. Courjal, M.-P. Bernal, A. Sabac, C. Bainier, and M. Spajer, Opt. Mater. **27**, 1421 (2005).

[8] F. Schrempel, T. Gischkat, H. Hartung, E.-B. Kley, and W. Wesch, Nucl. Instrum. Methods Phys. Res. B **250**, 164 (2006).

[9] F. Schrempel, T. Gischkat, H. Hartung, E. B. Kley, W. Wesch, and A. Tünnermann, in *Growth, Modification, and Analysis By Ion Beams at the Nanoscale*, edited by J. K. N. Lindner, M. Toulemonde, W. J. Weber, and B. L. Doyle, MRS Symposia Proceedings No. 908E (Material Research Society, Warrendale, PA, 2006), pp. 0908–OO16–01.

[10] M. R. Beghoul, B. Fougere, A. Boudrioua, C. Darraud, S. Latreche, R. Kremer, P. Moretti, and J. C. Vareille, Opt. Quantum Electron. **39**, 333 (2007).

[11] S. Diziain, J. Amet, F. I. Baida, and M.-P. Bernal, Appl. Phys. Lett. **93**, 261103 (2008).

[12] H. Hartung, R. Geiss, T. Gischkat, F. Schrempel, R. Iliew, T. Pertsch, F. Lederer, W. Wesch, E.-B. Kley, and A. Tünnermann, *IEEE/LEOS Winter Topicals Meeting Series* (IEEE/LEOS, Piscataway, NJ, USA, 2009), Vol. 2, p. TuA3.5.

[13] K. Sakoda and K. Ohtaka, Phys. Rev. B **54**, 5742 (1996).

[14] L. Tkeshelashvili and K. Busch, Appl. Phys. B: Lasers Opt. **81**, 225 (2005).

[15] M. W. McCutcheon, J. F. Young, G. W. Rieger, D. Dalacu, S. Frédérick, P. J. Poole, and R. L. Williams, Phys. Rev. B **76**, 245104 (2007).

[16] E. Centeno, D. Felbacq, and D. Cassagne, Phys. Rev. Lett. **98**, 263903 (2007).

[17] R. Iliew, C. Etrich, T. Pertsch, and F. Lederer, Phys. Rev. B **77**, 115124 (2008).

[18] F. Glöckler, S. Peters, U. Lemmer, and M. Gerken, Phys. Status Solidi A **204**, 3790 (2007).

[19] J. Amet, F. Baida, G. Burr, and M.-P. Bernal, Photonics Nanostruct. Fundam. Appl. **6**, 47 (2008).

[20] N. Kawai, K. Inoue, N. Carlsson, N. Ikeda, Y. Sugimoto, K. Asakawa, and T. Takemori, Phys. Rev. Lett. **86**, 2289 (2001).

[21] O. Painter, R. K. Lee, A. Scherer, A. Yariv, J. D. O'Brien, P. D. Dapkus, and I. Kim, Science **284**, 1819 (1999).

[22] B. Ben Bakir, C. Seassal, X. Letartre, P. Regreny, M. Gendry, P. Viktorovitch, M. Zussy, L. D. Cioccio, and J.-M. Fedeli, Opt. Express **14**, 9269 (2006).

[23] B. Ben Bakir, C. Seassal, X. Letartre, P. Viktorovitch, M. Zussy, L. D. Cioccio, and J. M. Fedeli, Appl. Phys. Lett. **88**, 081113 (2006).

[24] T.-C. Lu, S.-W. Chen, L.-F. Lin, T.-T. Kao, C.-C. Kao, P. Yu, H.-C. Kuo, S.-C. Wang, and S. Fan, Appl. Phys. Lett. **92**, 011129 (2008).

[25] M. A. Duguay, Y. Kokubun, T. L. Koch, and L. Pfeiffer, Appl. Phys. Lett. **49**, 13 (1986).

[26] R. Ferrini, A. Berrier, L. A. Dunbar, R. Houdré, M. Mulot, S. Anand, S. de Rossi, and A. Talneau, Appl. Phys. Lett. **85**, 3998 (2004).

[27] A. Taflove and S. C. Hagness, *Computational Electrodynamics: The Finite-Difference Time-Domain Method* (Artech House, Boston, MA, 2005).

[28] E. Chow, S. Lin, S. Johnson, P. Villeneuve, J. Joannopoulos, J. Wendt, G. Vawter, W. Zubrzycki, H. Hou, and A. Alleman, Na-

ture (London) **507**, 983 (2000).

[29] A. Chutinan, M. Okano, and S. Noda, Appl. Phys. Lett. **80**, 1698 (2002).

[30] S. Fan, S. G. Johnson, J. D. Joannopoulos, C. Manolatou, and H. A. Haus, J. Opt. Soc. Am. B **18**, 162 (2001).

[31] J. Witzens, T. Baehr-Jones, M. Hochberg, M. Lončar, and A. Scherer, J. Opt. Soc. Am. A **20**, 1963 (2003).

[32] P. Bienstman, S. Assefa, S. G. Johnson, J. D. Joannopoulos, G. S. Petrich, and L. A. Kolodziejski, J. Opt. Soc. Am. B **20**, 1817 (2003).

[33] A. Lavrinenko, P. Borel, L. Frandsen, M. Thorhauge, A. Harpøth, M. Kristensen, T. Niemi, and H. Chong, Opt. Express **12**, 234 (2004).

[34] R. Iliew, C. Etrich, U. Peschel, F. Lederer, M. Augustin, H.-J. Fuchs, D. Schelle, E.-B. Kley, S. Nolte, and A. Tünnermann, Appl. Phys. Lett. **85**, 5854 (2004).

[35] A. Mekis, S. Fan, and J. D. Joannopoulos, IEEE Microw. Guid. Wave Lett. **9**, 502 (1999).

[36] M. Koshiba, Y. Tsuji, and S. Sasaki, IEEE Microw. Wirel. Compon. Lett. **11**, 152 (2001).

[37] P. Lalanne, IEEE J. Quantum Electron. **38**, 800 (2002).

[38] G. R. Hadley, IEEE Photon. Technol. Lett. **14**, 642 (2002).

[39] L. C. Andreani and D. Gerace, Phys. Rev. B **73**, 235114 (2006).

[40] J. Jin, *The Finite Element Method in Electromagnetics*, 2nd ed. (John Wiley & Sons, New York, 2002).

[41] K. Beilenhoff, W. Heinrich, and H. L. Hartnagel, IEEE Trans. Microwave Theory Tech. **40**, 540 (1992).

[42] T. Ochiai and K. Sakoda, Phys. Rev. B **64**, 045108 (2001).

[43] L. C. Andreani and M. Agio, Appl. Phys. Lett. **82**, 2011 (2003).

[44] N. Moll and G.-L. Bona, J. Appl. Phys. **93**, 4986 (2003).

[45] L. C. Andreani, D. Gerace, and M. Agio, Photonics Nanostruct. Fundam. Appl. **2**, 103 (2004).

[46] G. P. Agrawal and N. K. Dutta, *Semiconductor Lasers* (Van Nostrand Reinhold, New York, 1993).

[47] L. A. Coldren and S. W. Corzine, *Diode Lasers and Photonic Integrated Cicuits* (John Wiley & Sons, New York, 1995).

[48] T. Ochiai and K. Sakoda, Phys. Rev. B **63**, 125107 (2001).

[49] P. Yeh, J. Opt. Soc. Am. **69**, 742 (1979).

[50] D. Michaelis, U. Peschel, C. Wächter, and A. Bräuer, Phys. Rev. E **68**, 065601(R) (2003).

[51] M. Notomi, K. Yamada, A. Shinya, J. Takahashi, C. Takahashi, and I. Yokohama, Phys. Rev. Lett. **87**, 253902 (2001).

[52] D. Mori and T. Baba, Opt. Express **13**, 9398 (2005).

[53] H. Gersen, T. J. Karle, R. J. P. Engelen, W. Bogaerts, J. P. Korterik, N. F. van Hulst, T. F. Krauss, and L. Kuipers, Phys. Rev. Lett. **94**, 073903 (2005).

[54] M. Qiu, Phys. Rev. B **66**, 033103 (2002).

[55] S. Olivier, M. Rattier, H. Benisty, C. Weisbuch, C. J. M. Smith, R. M. De La Rue, T. F. Krauss, U. Oesterle, and R. Houdré, Phys. Rev. B **63**, 113311 (2001).

[56] S. Olivier, H. Benisty, C. Weisbuch, C. J. M. Smith, T. F. Krauss, and R. Houdré, Opt. Express **11**, 1490 (2003).

[57] M. Augustin, R. Iliew, C. Etrich, F. Setzpfandt, H.-J. Fuchs, E.-B. Kley, S. Nolte, T. Pertsch, F. Lederer, and A. Tünnermann, New J. Phys. **8**, 210 (2006).

[58] M. Augustin, H.-J. Fuchs, D. Schelle, E.-B. Kley, S. Nolte, A. Tünnermann, R. Iliew, C. Etrich, U. Peschel, and F. Lederer, Appl. Phys. Lett. **84**, 663 (2004).